Decontamination of Sulfur Mustard on Manganese Oxide Nanostructures

G. K. Prasad, T. H. Mahato, Beer Singh, P. Pandey, A. N. Rao, K. Ganesan, and R. Vijayraghavan
Defense Research and Development Establishment, Jhansi Road, Gwalior 474002, India

DOI 10.1002/aic.11182
Published online April 16, 2007 in Wiley InterScience (www.interscience.wiley.com).

Nanostructures made up of restacked manganese oxide nanosheets and nanotubes were tested as reactive sorbents for the detoxification of sulfur mustard, a highly persistent and a deadly chemical warfare agent. The kinetic data was compared with that of the precursor bulk H_xMnO_2 material and the data show that the agent undergoes hydrolysis and elimination reactions and yields hemisulfur mustard, thiodiglycol, chlorovinylethyl sulfide, divinyl sulfide, and hydroxyvinylethyl sulfide on the surface of the adsorbent made up of nanosheets and tubes; however, it undergoes oxidation reaction and yields sulfoxide of sulfur mustard on the surface of bulk H_xMnO_2 material. Kinetic data reveal that the adsorbent compiled of manganese oxide nanosheets and nanotubes show a reaction half life of 9.12 h, where the bulk H_xMnO_2 show the reaction half life of 29.8 h. © 2007 American Institute of Chemical Engineers *AIChE J,* 53: 1562–1567, 2007
Keywords: nanostructures, detoxification, sulfur mustard, nanosheets and nanotubes

Introduction

Decontamination of the persistent (low volatile and high boiling) chemical warfare agents such as sulfur mustard becomes a major challenge for the researchers, as it remains in the environment even after longer intervals of time and poses threat to the exposed individual and environment. Of many formulations available till date, adsorbents composed of nanomaterials have been considered to be the potential materials for the decontamination applications,[1–7] Recently, nanosized inorganic oxide particles such as MgO, CaO, and Al_2O_3 were found to be the promising materials for the decontamination of chemical warfare agents.[8,9] They possessed enhanced reactivity toward the CW agents due to their large surface area and reactive edges, corner defects and unusual lattice planes relative to the conventional materials.[10–14] However, the nanocrystals or nanoparticles have a tendency to get aggregated and owing to this, some of the available active sites on the surface are not accessible to the adsorbate molecules. However, one of the variants of these nanomaterials, i.e., nanotubes or nanosheets, aggregate with each other typically without losing their surface area, thereby promising the accessibility to the adsorbate molecules toward the active sites. This typical interaction was attributed to the fact that the nanotubular materials orient/aggregate peculiarly to avoid electrostatic and steric repulsions of residual charges present over their surface.

Recently, the nanotubes based on TiO_2, MnO_2, $Ca_3Nb_3O_{10}$, and $K_{4-x}H_xNb_6O_{17}$ were synthesized from their respective nanosheet solutions by changing their ionic strength.[15] In addition to these, Kasuga et al.[16,17] and Chen et al.[18] prepared titania nanotubes by hydrothermal method. TiO_2 nanotubes have got immense importance because of their potential photocatalytic properties and chemical warfare (CW) agent decontamination properties and were successfully used in the decontamination of 2-chloroethyl ethyl sulfide (CEES), a well-known surrogate of deadly chemical warfare agent, i.e., sulfur mustard (HD).[19] This agent was found to get degraded on the surface of TiO_2 nanotubes by means of hydrolysis reactions. Other than this, no other chemical warfare agent decontamination studies were reported so far on other metal oxide nanotubes.

On the other hand, recently MnO_2 nanotubes with an outer diameter ~15 nm were prepared by changing the ionic

Correspondence concerning this article should be addressed to G. K. Prasad at gkprasad@lycos.com.

strength of the MnO_2 nanosheet solutions facilitated by the addition of NaOH solutions.[15] Inspired by these, we have attempted to study the reactions of highly persistent sulfur mustard (HD) on the surface of the aggregates of nanotubules and restacked nanosheets of MnO_2 and the data was compared with that of the bulk H_xMnO_2. After their synthesis, these materials were characterized by XRD, SEM-EDAX, N_2-BET, TG, and TEM techniques. Obtained materials were used to study the reactions with sulfur mustard and the progress of reaction was monitored by GC-FID; however, the degradation products were characterized by GC-MS.

Experimental

Materials

Tetrabutyl ammonium hydroxide (TBAOH 40% solution in water), KCl, $KMnO_4$, HCl, chloroform, and acetonitrile were obtained from E. Merck India and Across Organics, Belgium. Sulfur mustard (HD) (more than 99% purity) was obtained from synthetic chemistry division of our establishment. It was synthesized by the Meyer method and distilled at 110°C under vacuum.[20] Caution: Sulfur mustard is a potential vesicant and must be handled by trained personnel with care by wearing suitable protective gear only.

Synthesis of reactive sorbent composed of MnO_2 nanosheets and nanotubes

The nanostructures composed of restacked nanosheets of MnO_2 and nanotubes (MnO_2 NT) were synthesized by the flocculation of MnO_2 nanosheet solutions using aqueous solutions of KCl.[15] Prior to this, the nanosheet solutions were prepared by the exfoliation treatment of layered H_xMnO_2 (1.0 g) with 2 M aqueous solutions of tetrabutyl ammonium hydroxide (TBAOH) as per a reported procedure.[15] Then, obtained nanosheets solution was centrifuged at 10,000 rpm for removing the unexfoliated H_xMnO_2, whereas the layered $HMnO_2$ was synthesized by the soft chemical treatment of K_xMnO_2 with 1 M hydrochloric acid solution, which further was synthesized by recently reported procedure.[21] After obtaining the nanosheet solutions (10 mg/mL), 50 mL of 1% KCl aqueous solution was added to it. Immediately after the addition, the exfoliated nanosheets get flocculated thus facilitating the formation of aggregates of nanotubes and restacked nanosheets of MnO_2. Thereafter, the precipitate was left for few hours under vibration-free conditions, it was separated by centrifugation and washing, and then it was air-dried for overnight.

Characterization of MnO_2 nanosheets and nanotubes

XRD patterns were obtained in an X Pert Pro Diffractometer, Panalytical, Netherlands, using Cu Kα radiation. SEM-EDAX measurements were done on a Philips instrument equipped with EDAX facility. TEM data was obtained on a JEOL transmission electron microscope 1200 EX. The samples were suspended in ethanol and sonicated for over 10 min. Subsequently, a drop of the supernatant dispersion was placed onto a carbon film supported by a copper grid. N_2 BET measurements were done on Sorptomatic 1990 Fison instrument, Italy make. Subsequently, thermograms were recorded on TGA-2950, TA instruments, USA. The Chemito 8610 gas chromatograph equipped with FID detector and BP10 column (30 m length, 0.5 mm i.d.) was used for the degradation kinetics of HD, whereas HP Agilent GC-MS system (5973 Inert) was used for the characterization of reaction products.

Results and Discussion

Flocculation of the colloidal dispersion of MnO_2 nanosheets by adding KCl solutions facilitated the formation of novel mesoporous adsorbent composed of nanostructures (nanotubes and restacked MnO_2 nanosheets) (MnO_2 NT) and is shown in Figure 1. The figure shows the aggregates of nanosheet materials that are randomly oriented and irregularly stacked by yielding house of cards like porous structure. The N_2 BET investigations on the material revealed that it exhibits a slightly different Type IV adsorption isotherm with a hysteresis (H3-type) typical of slit-shaped mesopores as per IUPAC nomenclature as illustrated in Figure 2a. The pore size distribution (Figure 2b) of the material obtained by BJH method indicates the same with pore maxima at ~5.0 nm. The surface area and pore volume are found to be 187 m^2/g and 0.2 mL/g. This considerable amount of surface area can be ascribed to the random orientation of nanotubes without loosing the connectivity within their tips and the randomly restacked nanosheets by yielding house of cards structure with slit-type of mesopores. Subsequently, the material was characterized also by transmission electron microscopy and the data is illustrated in Figures 3a,b. Figure 3a depicts needle-shaped crystallites and it also illustrates that the needle-like materials are expected to be formed due to lateral curling of nanosheets of MnO_2. Electron micrographs (not shown here) taken at still higher magnification illustrated the hollowness within their core and the scale on the micrographs revealed the outer and internal diameters of the nanotubes to be ranging from 10 to 15 nm and from 3 to 5 nm, respectively, and the data is consistent with the previously reported

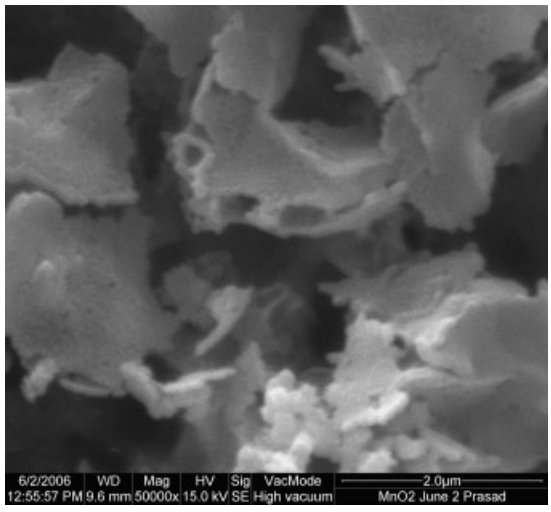

Figure 1. Scanning electron micrograph of the reactive sorbent composed of restacked MnO_2 nanosheets and nanotubes.

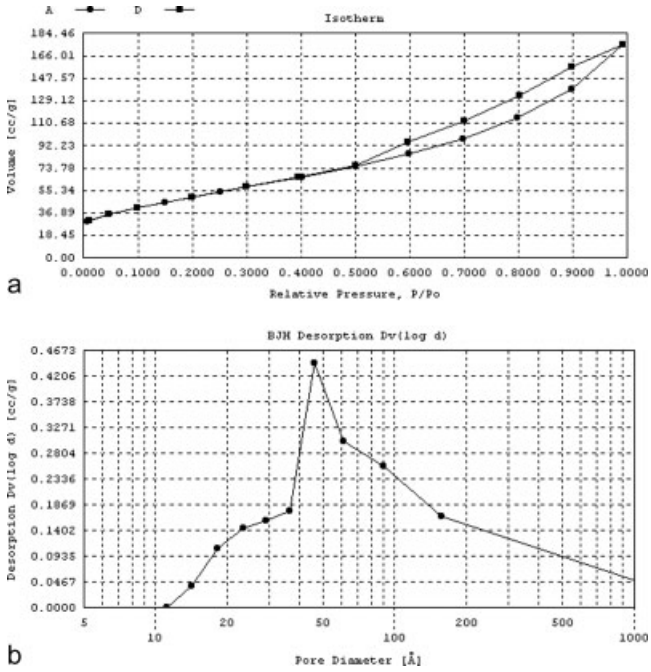

Figure 2. Nitrogen adsorption isotherm (a) and pore size distribution (b) of the reactive sorbent (MnO_2).

data.[15] The solutions containing nanosheets were made initially by the exfoliation treatment of the H_xMnO_2 of bulk size (micron-sized) with the aqueous solutions of tetrabutyl ammonium hydroxide. The formation of nanotubes from nanosheet solutions can be attributed to the ion exchange process. The abrupt addition of K^+ ions to the nanosheet solutions causes the restacking of MnO_2 nanosheets; however, during the washing process, some amount of restacked nanosheets again get delaminated and during this process, the K^+ ions and water molecules present at the edges of nanosheet exchange with each other thereby creating charge and steric imbalance within the nanosheet. Owing to this, they curl to form the nanotubes and the same was consistent with the previously reported results.[15] In addition to the tubes, the unrolled microsized (1–3 μm) sheets with thickness at around 0.7–0.8 nm were also observed and are also illustrated in Figure 3. Later, obtained material was characterized by X-ray diffraction technique and the data is shown in Figure 4. It shows broad peaks at 2θ of 12.2, 24.8, 36.3°, which can be attributed to the structure similar to the perturbed δ MnO_2. The broadness of peaks can be ascribed to the lack of three-dimensional order in the layered phase, which is expected to arise due to the irregularly restacked nanosheets encapsulated with water and K^+ ions. Presence of K^+ ions within the materials was confirmed by EDAX data and is illustrated in Table 1. It reveals that, 32.72 wt % of oxygen, 7.71 wt% potassium, and 48.56 wt % manganese were found to be present in the aggregate material besides the 0.24 wt % of Si and 1.38 wt % of chlorine as impurities, and the composition of the nanostructures was estimated to be $K_{0.19}Mn_{0.88}O_{2.05}$. In addition to these restacked materials, the nanoscrolls/tubes those were formed during the ion exchange

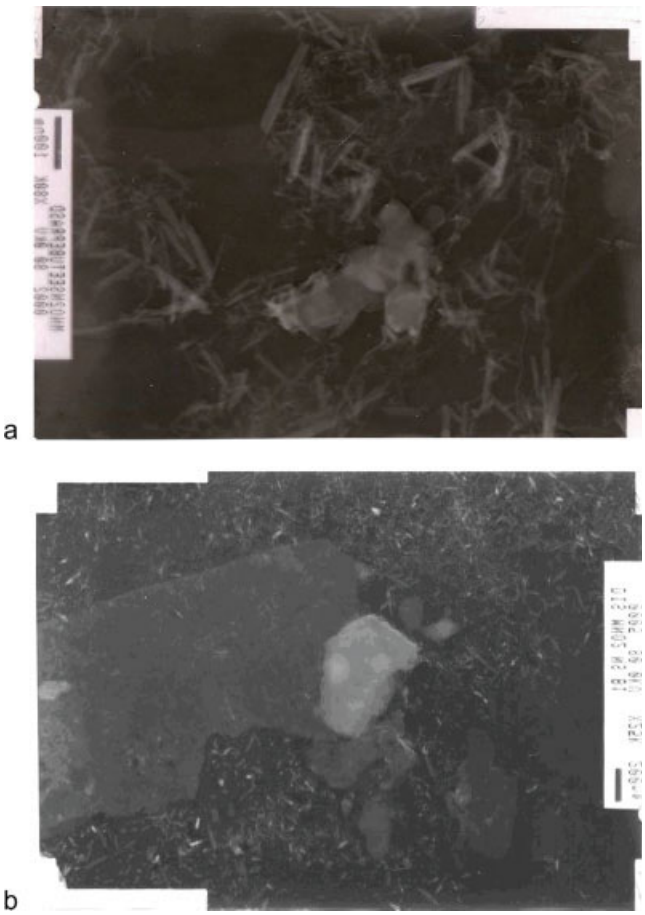

Figure 3. Transmission electron micrograph of the sorbent composed of MnO_2 nanotubes (a) and nanosheets (b) (scale 100 nm).

[Color figure can be viewed in the online issue, which is available at www.interscience.wiley.com.]

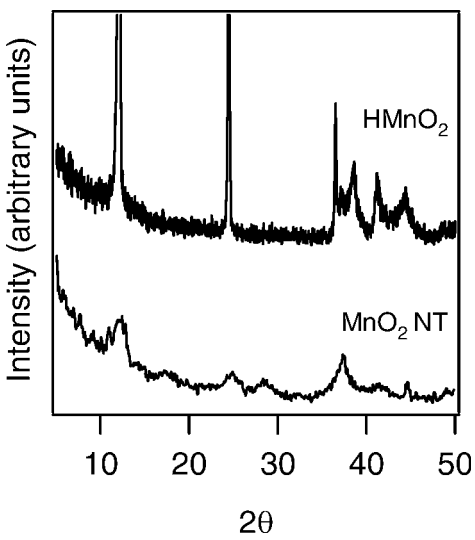

Figure 4. X-ray diffraction patterns of the reactive sorbent composed of MnO_2 restacked nanosheets and nanotubes and bulk H_xMnO_2.

Table 1. EDAX Data of the Aggregate Based on MnO_2 Nanosheets and Nanotubes/Nanostructures

Element	Wt %	At %
OK	32.72	51.70
SiK	0.24	0.22
ClK	1.38	0.98
KK	7.71	4.98
MnK	48.56	22.34

process as stated above are also expected to possess an interwall separation of 0.73 nm (2θ of 12.2°) (should not be confused with tube diameter). For comparison, we also have measured the XRD data for the bulk H_xMnO_2, which was obtained by the soft chemical treatment of K_xMnO_2. The XRD data show the sharp peaks at 2θ of 12.2, 24.8, 36.3°, which can be attributed to the δ MnO_2 structure in which the ordered MnO_2 layers are balanced by H^+ ions and is consistent with the previously reported results.[21]

Obtained mesoporous adsorbent composed of MnO_2 nanostructures was used to study the reaction with sulfur mustard (HD) at room temperature (35°C) and the data was compared with that of the bulk H_xMnO_2. For this purpose, 100 μL of chloroform solution having 2 μL of HD was added to 100 mg of the above adsorbent powder in a dropwise manner with the help of a micropipette and then the mixture was stirred magnetically for few seconds to ensure contact with entire powder and the remaining HD was extracted by acetonitrile at periodic intervals of time until 120 h to study the kinetics of degradation. For each time interval, the residual HD was extracted by using 5.0 mL of acetonitrile for five times to (each time 1 mL) ensure the complete extraction. Obtained solutions were *quantitatively* analyzed by gas chromatograph equipped with flame ionization detector under isothermal conditions at 110°C. As per GC data, sulfur mustard was eluted at 3.2 min and all the reaction mixtures extracted from the HD-exposed MnO_2 nanostructures at kinetic intervals of time were quantitatively analyzed by calibrating the concentrations. Subsequently, obtained kinetic data was plotted by taking $\log(a/(a - x))$ (a is initial HD concentration and $a - x$ is HD concentration at time t hours) on Y-axis and time on X-axis and the graph is depicted in Figure 5. The figure depicts the linear curve with fast initial reaction and a steady state at later stages of the reaction with a rate constant of 0.076 h^{-1} and half life of 9.12 h, thus indicating the pseudo first order behavior of decontamination reaction of HD on MnO_2 nanostructures,[22–24] whereas bulk H_xMnO_2 exhibits a rate constant of 0.0232 h^{-1} and half life of 29.8 h. The rate of decontamination reaction of HD on the surface of aggregates of restacked MnO_2 nanosheets and nanotubes is higher than the rate on the surface of bulk material, where, half life of the reaction is smaller than for nanoaggregates and bulk material, respectively. This observation can be attributed to two facts, one is the surface area available on nanoaggregates, i.e., 187 m^2/g, which is noticeably higher than the surface area of bulk H_xMnO_2, i.e., 40 m^2/g (the adsorption isotherm of the same is not provided). Most likely, owing to the higher surface area, more amount of HD is adsorbed on the surface and reacted with the relatively larger number of reactive site available within the nanoaggregates when compared with the bulk material. Preferably, the intercalated/physisorbed water molecules and the other intrinsic materials present within the nanoaggregates could have played the interesting role as active sites for the decontamination reactions. Moreover, the experiment was repeated several times to ensure the reproducibility of the kinetic data.

On the other facet, the fast initial reaction can be ascribed to the distribution of the liquid within the pores and its interaction with the accessible reactive sites. The limited surface reaction occurs when the sites are exhausted, obviously, replacing the initial fast reaction by a steady state reaction (steady state reaches in 72 h). This fact is supported also by the observation that, the concentration of products increased as a function of time and the GC MS data revealed the formation of elimination and oxidation products at the initial stages of the reaction, i.e., the fast initial reaction and the hydrolysis products at the steady state, i.e., slower hydrolysis reaction. These observations can be attributed to the high surface area available in the case of nanoaggregates relative to bulk material, or the consumption of the active sites.

Thereafter, the reaction mixtures obtained from the MnO_2 NT, i.e., the nanoaggregate and the bulk H_xMnO_2, were analyzed by GC-MS for the characterization of reaction products and the data was verified for product fragmentation patterns based on matches with the NIH databases. Data obtained for one of the products, illustrates the m/z values at 122, 104, 91, 75, 61, and 45, thus indicating the formation of thiodiglycol (TDG) and further emphasizing the role of hydrolysis reaction in the decontamination of HD to TDG thereby rendering it nontoxic. In addition to the hydrolysis product, elimination products 2-hydroxyethylvinyl sulfide and divinyl sulfide were also observed with m/z values at 104, 73, 61, and 59; 85, 71, 59, and 53, respectively as per the GC-MS data. In addition to these, residual HD was also identified with the m/z values at 158, 109, 73, 63, and 45. The reaction scheme of HD during hydrolysis reaction is also proposed and is depicted in Scheme 1. The occurrence of the hydrolysis reactions on the surface of the nanoaggregates can be attributed to their basic nature and are analogous to solution chemistry of the sulfur mustard.[2] Under this basic pH, the

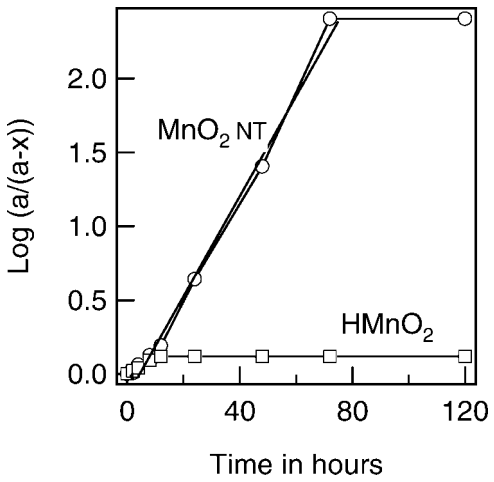

Figure 5. Kinetics of degradation reaction of HD on the adsorbent composed of MnO_2 nanosheets and nanotubes and bulk H_xMnO_2.

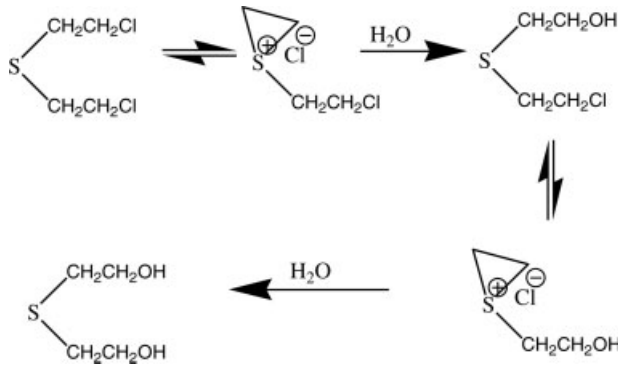

Scheme 1. The hydrolysis reactions of sulfur mustard on the surface of MnO_2 nanoaggregates.

physisorbed water or encapsulated water molecules could have effected the hydrolysis and elimination reactions of the sulfur mustard thereby rendering it nontoxic (no excess water was added prior to the reaction). Most likely, the cyclic sulfonium cation-Cl^- anion is formed initially as depicted in the above scheme and it is relatively unstable, because of which it could not be extracted and detected. Subsequently, the sulfonium ion interacts with water molecules present within the MnO_2 nanostructures to form the TDG. However, the formation of 2-hydroxyethylvinyl sulfide and divinyl sulfide is explained in Scheme 2. Most likely, the 2-chloroethylvinyl sulfide appears to be formed by the removal of HCl due to the elimination reaction and then the vinyl product got transformed to sulfonium ion, which further got hydrolyzed by water molecules to form 2-hydroxyethylvinyl sulfide, whereas the 2-chloroethylvinyl sulfide was transformed further to divinyl sulfide by the elimination of one more HCl.

Being a potential oxidant, manganese oxide present in the form of nanoaggregates could not oxidize the sulfur mustard to its oxidation products. This observation can be ascribed to

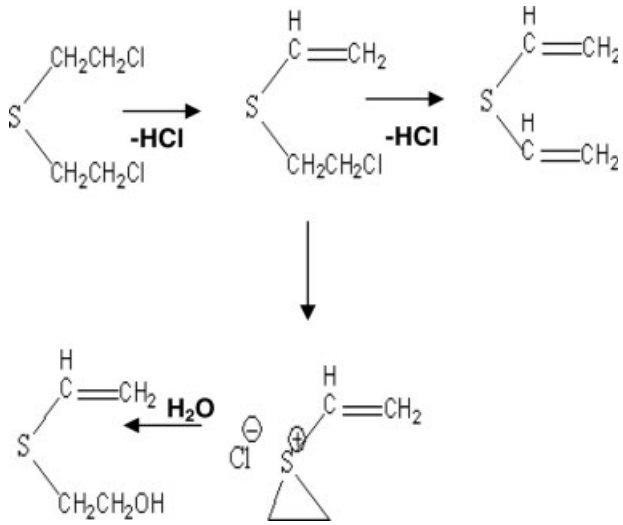

Scheme 2. The elimination reactions of sulfur mustard on the surface of MnO_2 nanoaggregates.

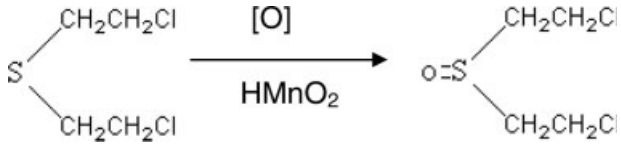

Scheme 3. The reactions of sulfur mustard on the surface of bulk $HMnO_2$.

two reasons; one is the predominant formation of relatively unstable sulfonium ion due to the release of chloride ion, which further reacted with water to form the hydrolysis product,[25] and the other is the poisoning of the required sites or functional groups on the surface of nanostructures (MnO_2 NT), which are responsible for oxidation reaction. To find out the amount of water in the nanoaggregate of MnO_2, it was subjected to thermogravimetric analysis. The data exhibited a weight loss of 10% after heating up to 150°C and it can be attributed to the loss of water that was present within the intercalated spaces of nanosheet and nanotube aggregates, where the bulk H_xMnO_2 exhibited a weight loss of 5% when heated up to 150°C, which can be attributed to the intercalated water (no excess water was added to the materials prior to the reactions). In contrary to the above observations, bulk H_xMnO_2 exhibited oxidation product of sulfur mustard, i.e., sulfoxide of mustard. The *m/z* values of the reaction mixture obtained from H_xMnO_2 exposed to sulfur mustard were 174, 112, 83, 76, and 63. Formation of sulfoxide (Scheme 3) on the surface of the bulk H_xMnO_2 can be ascribed to acidic nature of the surface and is analogous to the solution chemistry of the agent.[2] Moreover, the bulk H_xMnO_2 was prepared by the soft chemical treatment of K_xMnO_2 with hydrochloric acid solutions, although, after the treatment the final product was washed extensively with water, it contains the H^+ and some intercalated water. In the presence of the intercalated water and H^+ ions, the available functional groups on manganese oxide could have facilitated the oxidation of the sulfur mustard up to a certain extent; however, the surface area available is very low when compared with the nanoaggregates/structures, owing to this the amount of water and functional groups present within bulk H_xMnO_2 is low, thereby exhibiting slower detoxification reaction of the sulfur mustard. The same was reflected in the smaller rate constant value relative to nanoaggregates. Collectively, the nanoaggregates offer large surface area and facilitate the adsorption and encapsulation of the agent. And then, water present in the intercalated spaces will react with the agent thereby rendering the toxic agent to nontoxic. These results show that, the nanostructures of MnO_2 exhibit promising results on par with the existing solid decontamination systems such as nanosized MgO, Al_2O_3, etc.[1–12] Nanosized MgO and Al_2O_3 exhibited relatively lower reactivity than the nanoaggregates of MnO_2 emphasizing the potentiality of the MnO_2 nanoaggregates for the decontamination of persistent chemical warfare agents.

Conclusion

A Novel mesoporous adsorbent based on the nanostructures/aggregates of MnO_2 was synthesized and characterized.

Thereafter, it was used for studying the decontamination reaction with sulfur mustard, a chemical warfare agent, and the data was compared with that of the bulk H_xMnO_2. The results show that the adsorbent composed of MnO_2 nanoaggregates is promising for the decontamination of sulfur mustard as it could destroy the agent by the pseudo first-order steady-state reaction (hydrolysis and elimination) with a half life of 9.12 h, whereas the bulk H_xMnO_2 reacts with a half life of 29.8 h. Although, the bulk material destroys the agent, the detoxification reaction is slower than that occurring on the surface of nanoaggregates. So, these materials can be used for the decontamination of persistent CW agents.

Acknowledgments

We would like to thank Dr. P. K. Gutch and Amit Saxena for the timely help and encouragement.

Literature Cited

1. Wagner GW, Procell LR, O'Connor RJ, Shekar M, Carnes CL, Kapoor PN, Klabunde KJ. Reactions of VX, GB, GD and HD with nanosize Al_2O_3. Formation of aluminiumphosphates. *J Am Chem Soc*. 2001;123:1636–1644.
2. Yang Y-C, Baker JA, Ward JR. Decontamination of chemical warfare agents. *Chem Rev*. 1992;92:1729–1743.
3. Yang Y-C. Chemical reactions for neutralizing chemical warfare agents. *Chem Ind*. 1995;9:334–337.
4. Ekerdt JG, Klabunde KJ, Shapley JR, White JM, Yates JT. Surface chemistry of organophosphorous compounds. *J Phys Chem*. 1988;92:6182–6188.
5. Mawhinney DB, Rossin JA, Gehart K, Yates JT. Adsorption and reaction of 2–chloroethylethyl sulfide with Al_2O_3 surfaces. *Langmuir*. 1999;15:4789–4795.
6. Wagner GW, Bartram PW, Koper O, Klabunde KJ. Reactions of VX, GD and HD with nanosize MgO. *J Phys Chem B*. 1999;103:3225–3228.
7. Wagner GW, Bartram PW. Interaction of VX, G and HD simulants with self decontaminating sorbents. A solid state NMR study. ERDEC-TR-375, Aberdeen Proving Ground, MD, 1996.
8. Stark JV, Park DG, Lagadic I, Klabunde KJ. Nanoscale metal oxide particle/clusters as chemical reagents. Unique surface chemistry on magnesium oxide as shown by enhanced adsorption of acid gases (sulfur oxide and carbon dioxide) and pressure dependence. *Chem Mater*. 1996;8:1904–1912.
9. Bartram PW, Wagner GW. Decontamination of chemical warfare agents using activated aluminium oxide. US Patent No. 5689038, Nov 18, 1997.
10. Klabunde KJ, Stark J, Koper O, Mohs C, Park DG, Decker S, Jiang Y Lagadic, Zhang D. Nanocrystals as stoichiometric reagents with unique surface chemistry. *J Phys Chem*. 1996;100:12142.
11. Sides GD, Mason DW, Seiders RP. Interaction of the agents HD, GD and VX with alumina. In Proceedings of the 1983 scientific conference on chemical defense research, CRDC-SP-84014; Aberdeed Proving Ground, MD, 1984:285–291.
12. Wagner GW, Bartram PW. Reactions of mustard stimulant 2–chloroethylphenyl sulphide on self decontaminating sorbent. A ^{13}C NMR study. *J Mol Catal A: Chem*. 1996;111:175–180.
13. Wagner GW, Bartram PW. ^{31}P MAS NMR study of the hydrolysis of O,S-diethyl phenyl phosphonothioate on reactive sorbents. *J Mol Catal A:Chem*. 1995;99:175–181.
14. Wagner GW, Koper O, Lucas E, Decker S, Klabunde KJ. Reactions of VX, GD and HD with nanosize CaO: Autocatalytic dehydrohalogenation of HD. *J Phys Chem B*. 2000;104:5118–5123.
15. Ma R, Bando Y, Sasaki T. Directly rolling nanosheets into nanotubes. *J Phys Chem*. 2004;108:2115–2119.
16. Kasuga T, Hiramatsu M, Hoson A, Sekino T, Nihara K. Formation of titanium oxide nanotube. *Langmuir*. 1998;14:3160–3163.
17. Kasuga T, Hiramatsu M, Hoson A, Sekino T, Nihara K. Titanate nanotubes prepared by chemical processing. *Adv Mater*. 1999;11:1307.
18. Chen Q, Zhou W, Du G, Peng L-M. Titanate nanotubes made via single alkali treatment. *Adv Mater*. 2002;14:1208–1211.
19. Kleinhammes A, Wagner GW, Kulkarni H, Jia Y, Zhang Qi, Qin L-C, Wu Y. Decontamination of 2–chloroethyl ethyl sulfide using titanate nanoscrolls. *Chem Phys Lett*. 2005;411:81–85.
20. Franke S. Lehrbuch der Militarchemie, Vol. 1, Militarverlag der DDR, Berlin, 1977.
21. Komaba S, Kumagai N, Chiba S. Synthesis of layered MnO_2 by calcinations of $KMnO_4$ for rechargeable lithium battery cathode. *Electrochim Acta*. 2000;46:31–37.
22. Hinshelwood CN. *The Kinetics of Chemical Change*. London: Oxford University Press, 1940:206–209.
23. Laidler KJ. *Chemical Kinetics*. New York: McGraw-Hill, 1950.
24. Maron SH, Prutton CF. *Principles of Physical Chemistry*, 4th ed. New Delhi, India: Amerind Publishing, 1972:548–592.
25. Yang YC, Szafraniec LL, Beaudry WT, Richard JW. Kinetics and mechanism of the hydrolysis of 2 chloro ethyl sulfides. *J Org Chem*. 1988;53:3293–3297.

Manuscript received Feb. 22, 2007, and revision received Mar. 13, 2007.